Received June 3, 2020, accepted June 15, 2020, date of publication June 19, 2020, date of current version June 30, 2020.

Digital Object Identifier 10.1109/ACCESS.2020.3003655

FEM Simulation of Charge Accumulation Behaviours on Polyimide Surface in 10 kV Negative High-Voltage Corona Polarization Process

TAO FENG[1,2], WEI HE[1], AND JIN GANG WANG[1]

[1]State Key Laboratory of Power Transmission Equipment and System Security and New Technology, Chongqing University, Chongqing 400044, China
[2]College of Electrical Engineering, Shijiazhuang Tiedao University, Shijiazhuang 050043, China

Corresponding author: Wei He (hewei@cqu.edu.cn)

This work was supported by the National Natural Science Foundation of China under Grant 51677009.

ABSTRACT The study investigates behaviors of charge accumulation on an insulated surface from micro perspective via the numerical method. A coupling bridge between the micro-ion reaction system and the macroscopic multi-physical field was constructed by means of the electronic energy distribution function, which revealed the coupling mechanism in the process of corona charge. Moreover, it revealed the transport and accumulation mechanism of charge on the surface of insulating materials. 2D axisymmetric finite element model was built based on the multi-physical field coupling theory. 10 kV negative voltage was applied using a pin-plate electrode structure and polyimide film was taken as insulated surface to simulate the dynamic charge accumulation behaviors in the corona discharge process. The generation, migration and distribution laws of charged ions and electrons in different stages of corona discharge process were given. Charge distribution laws in different stages of charge process of polyimide were given and discussed. When corona discharge reached quasi-stationary state, the total charge number accumulated on the surface was at 10^{-10} Coulomb order of magnitude, and the drift current was at 10^{-7} ampere order of magnitude. An experimental platform was set up to test drift current and charge distribution under quasi-stable discharge state. The results show that the simulation results and the experimental data under quasi-stable state are consistent, thus indirectly verifying the correctness of the proposed numerical simulation algorithm and its simulation results.

INDEX TERMS Air gaps, charge transfer, finite element methods, surface charging.

I. INTRODUCTION

Surface charge plays a significant role in dielectric strength of solid-gas interface, especially for electrical equipment with complex 3D structures [1]. Surface charge accumulation can lead to drop of surface flashover voltage of insulator and degradation of breakdown characteristics of supporting insulator [2]. The hydrophobicity of silicon rubber insulation material will decline somehow under surface charge accumulation [3]. The aging and insulation failure of polymer insulation material is closely associated with surface charge accumulation and migration [4], [5]. Charge accumulation on solid insulated surface under continuous high-voltage DC stress has become a serious problem [6].

Many scholars have done a lot of research work regarding the effect of surface charge on dielectric strength at solid-gas interface and charge accumulation mechanism [1], [2], [7]–[15]. Due to the difference in factors like experimental conditions and research methods adopted by researchers, experimental results are usually inconsistent and they may even obtain totally opposite conclusions [11], leading to the lack of comprehensive understanding of dynamic charge accumulation behaviors and characteristics. The generation and accumulation process of surface charge of insulating medium is comprehensively influenced by various multi-physics factors. The scarce theoretical equations are all one-dimensional discharge equations on theoretical foundation of

The associate editor coordinating the review of this manuscript and approving it for publication was Boxue Du.

corona discharge [17]. It's hard for the existing theoretical equations to realize simulation computation of surface charge accumulation effect of insulating medium under the multi-structure multi-field coupling effect.

In this study, a coupling bridge between the micro-ion reaction system and the macroscopic multi-physical field (electric field, magnetic field, flow field, energy field, and heavy ion concentration field) was constructed by means of the electronic energy distribution function, which revealed the coupling mechanism in the process of corona charge. Moreover, it reveals the transport and accumulation mechanism of charge on the surface of insulating materials. 2D axisymmetric finite element model was established based on multi-scale and multi-physics coupling theory to simulate the air corona discharge polarization process. Finite element software was employed for modeling and simulation so as to analyze and explain the gas corona discharge phenomenon in atmospheric environment, give migration, transport and distribution of all kinds of charged particles at different time in the discharge process, probe into dynamic charge accumulation process on polyimide film surface and analyze the physical mechanism of charge accumulation. In the end, the correctness of simulation and theoretical analysis was verified indirectly by combining an experimental study under quasi-stable state. This study is expected to provide theoretical support for the leading mechanism to prevent discharge or flashover along the surface.

II. MATHEMATICAL MODEL

At micro level, Nano scale collision, ionization and adsorption problems between ion-ion, ion-electron, electron-neutral particle and ion-neutral particle can be explained using theories of molecular dynamics and electrodynamics. From macro-level, based on the reaction coefficients obtained through the above mentioned calculation, macro concentration distributions of all kinds of aforementioned ions, electrons and neutral particles nearby the discharge region can be calculated according to geometric fluid theory, electric field migration theory, etc.

A. IONIC REACTION IN AIR CORONA DISCHARGE

During the air corona discharge process, reaction types where electrons participate mainly include ionization, attachment, collision and excitation. There are many kinds of micro particles involved in the reaction, and the number of reaction equations involved is more than 100. Table 1 is a simplified equation list, which shows the reaction equations involved in atmospheric air corona discharge and their corresponding energy losses and reaction types. Table 1 is based on the following assumptions and analysisčžThe main gas components in air are oxygen and nitrogen, which account for 21% and 78%, respectively, and the rest accounts for 1% [18]. The reaction involved in the air corona discharge process can be approximately regarded as reaction of oxygen and nitrogen

TABLE 1. Ionic reaction equations of air corona discharge.

No.	Reaction equation	Energy loss (eV)	Reaction type
1	$E + N_2 \rightarrow E + N_2$	-	Effective
2	$E + N_2 \rightarrow E + N_2$ (v=0 - v=1)	0.3	Excitation
3	$E + N_2 \rightarrow E + N_2$ (v=0 - v=2)	0.6	Excitation
4	$E + N_2 \rightarrow E + N_2$ (v=0 - v=3)	0.9	Excitation
5	$E + N_2 \rightarrow E + N_2$ (v=0 - v=4)	1.1	Excitation
6	$E + N_2 \rightarrow E + N_2$ (v=0 - v=5)	1.4	Excitation
7	$E + N_2 \rightarrow E + N_2$ (v=0 - v=6)	1.7	Excitation
8	$E + N_2 \rightarrow E + N_2$ (v=0 - v=7)	2.0	Excitation
9	$E + N_2 \rightarrow E + N_2$ (v=0 - v=8)	2.2	Excitation
10	$E + N_2 \rightarrow E + N_2$ (v=0 - v=9)	2.5	Excitation
11	$E + N_2 \rightarrow E + N_2$ (v=0 - v=10)	2.7	Excitation
12	$E + N_2 \rightarrow E + N_2$ [A3Su+(v=0-4)]	6.2	Excitation
13	$E + N_2 \rightarrow E + N_2$ [A3Su+(v=5-9)]	7.0	Excitation
14	$E + N_2 \rightarrow E + N_2$(B3Pg)	7.4	Excitation
15	$E + N_2 \rightarrow E + N_2$(W3Du)	7.4	Excitation
16	$E + N_2 \rightarrow E + N_2$ [A3Su+(v=10+)]	7.8	Excitation
17	$E + N_2 \rightarrow E + N_2$(B3Su-)	8.2	Excitation
18	$E + N_2 \rightarrow E + N_2$(a1Su-)	8.4	Excitation
19	$E + N_2 \rightarrow E + N_2$(a1Pg)	8.6	Excitation
20	$E + N_2 \rightarrow E + N_2$(w1Du)	8.9	Excitation
21	$E + N_2 \rightarrow E + N_2$(C3Pu)	11.0	Excitation
22	$E + N_2 \rightarrow E + N_2$(E3Sg+)	11.8	Excitation
23	$E + N_2 \rightarrow E + N_2$(a1Sg+)	12.2	Excitation
24	$E + N_2 \rightarrow E + N_2$(sing-sup)	13.0	Excitation
25	$E + N_2 \rightarrow E + E + N_2^+$	15.6	Ionization
26	$E + O_2 \rightarrow O^- + O$	0	Attachment
27	$E + O_2 \rightarrow E + O_2$	-	Effective
28	$E + O_2 \rightarrow E + O_2$(v=0 - v=1)	0.19	Excitation
29	$E + O_2 \rightarrow E + O_2$(v=0 - v=2)	0.38	Excitation
30	$E + O_2 \rightarrow E + O_2$(v=0 - v=3)	0.6	Excitation
31	$E + O_2 \rightarrow E + O_2$(v=0 - v=4)	0.8	Excitation
32	$E + O_2 \rightarrow E + O_2$(a1Dg)	0.977	Excitation
33	$E + O_2 \rightarrow E + O_2$(b1Sg+)	1.627	Excitation
34	$E + O_2 \rightarrow E + O_2$ (A3Su+,C3Du,C1Su-)	4.5	Excitation
35	$E + O_2 \rightarrow E + O(3P)+O(3P)$	6.0	Excitation
36	$E + O_2 \rightarrow E + O(3P)+O(1D)$	8.4	Excitation
37	$E + O_2 \rightarrow E + O_2$(9.97eV)	9.97	Excitation
38	$E + O_2 \rightarrow E + O_2$(14.7eV)	14.7	Excitation
39	$E + O_2 \rightarrow E + E + O_2^+$	12.1	Ionization

TABLE 2. Reduced ionic reaction equations of air corona discharge.

No.	Reaction equation	Energy loss (eV)	Reaction type
1	e +A=>p+2e	15	Ionization
2	e +A=>n	-	Adhesion
3	e +2A=>n+A	-	Adhesion
4	e +p=>A	-	Chemical reaction
5	n + p => 2A	-	Chemical reaction

with their derivative ions. As can be seen from Table 1, even so simplified, the number of equations involving the micro reaction of oxygen and nitrogen with their derivative ions is still as high as 39 [19]–[21]. The more the number of reaction equations, the more unfavorable it is to the convergence of the solution of mathematical model. At present, the data of collision cross section under high voltage and high electric field energy in the database are not complete. To obtain these data, we have to expand the existing data linearly, which is not conducive to the convergence of the equation solution. In consideration of complexity of numerous reaction equations and their effect on convergence of numerical equations, drawing on the model proposed by Professor Kulikovsky [22], the air can be regarded as a mixed plasma system consisting of neutral particle A, positive ion p, negative ion n and electron e. Then we can get the reduced ionization reaction equations shown in Table 2 to describe the air corona discharge process under normal pressure.

Electron source items of reaction equations in Table 2 can be respectively characterized as follows [20], [21]:

$$R_{\mathrm{e},1} = x_{\mathrm{A}1}\alpha_{\mathrm{A}1}N_{\mathrm{A}1}n_{\mathrm{e}1} \tag{1}$$

where $R_{\mathrm{e},1}$, $x_{\mathrm{A}1}$, $\alpha_{\mathrm{A}1}$, $N_{\mathrm{A}1}$ and $n_{\mathrm{e}1}$ are the electron source term, molar percentage of neutral particle A, Townsend discharge coefficient, neutral particle number concentration and electron molar concentration of ionizing reaction equation (1), respectively. The relation between Townsend discharge coefficient $\alpha_{\mathrm{A}1}$ and average electron energy is acquired through the experiment [20] as shown in Figure 1.

$$R_{\mathrm{e},2} = x_{\mathrm{A}2}\alpha_{\mathrm{A}2}N_{\mathrm{A}2}n_{\mathrm{e}2} \tag{2}$$

where $R_{\mathrm{e},2}$, $x_{\mathrm{A}2}$, $\alpha_{\mathrm{A}2}$, $N_{\mathrm{A}2}$ and $n_{\mathrm{e}2}$ are the electron source term, molar percentage of neutral particle A, Townsend discharge coefficient, neutral particle number concentration and electron molar concentration of reaction equation (2), respectively. The relation between Townsend discharge coefficient $\alpha_{\mathrm{A}2}$ and average electron energy is acquired through the experiment [20] as shown in Figure 2.

$$R_{e,3} = x_{A3}k_3N_{A3}n_{e3} \tag{3}$$

where $R_{e,3}$, x_{A3}, k_3, N_{A3} and n_{e3} are the electron source term, molar percentage of neutral particle A, three-body reaction rate with electron temperature dependence, neutral particle number concentration and electron molar concentration of reaction equation 3, respectively. Based on the Arrhenius equation, the reaction rate k_3 considering the influence of

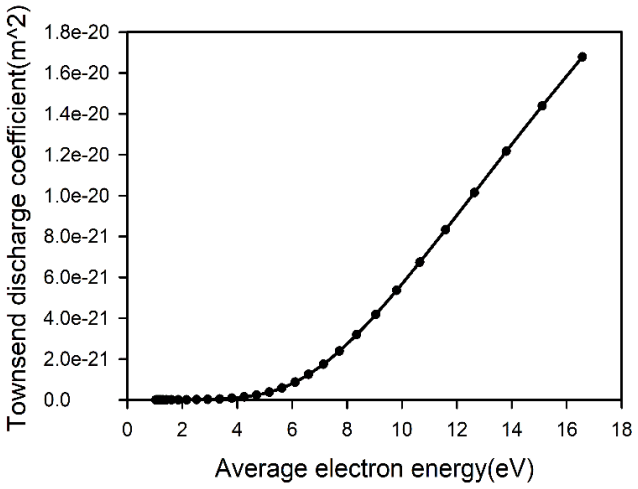

FIGURE 1. Relation between Townsend discharge coefficient and average electron energy in ionization reaction equation 1.

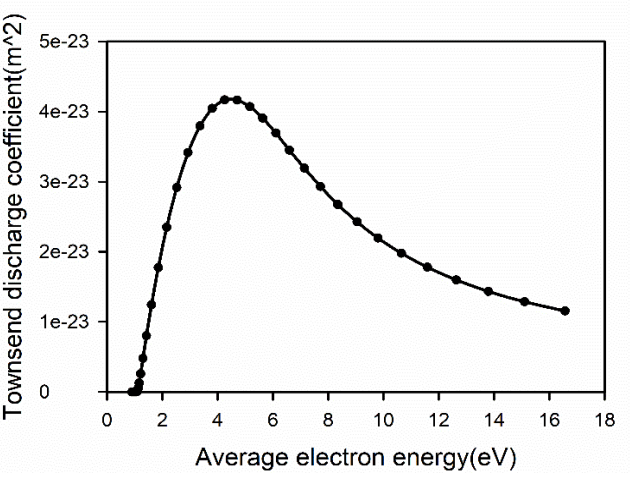

FIGURE 2. Relation between Townsend discharge coefficient and average electron energy in complex reaction equation 2.

temperature is introduced. The fitted expression according to the experiment is:

$$k_3 = 1.4 \times 10^{-42}\frac{0.026}{T_e}e^{(\frac{100}{T_{gas}}-\frac{0.061}{T_e})}N_A^2 \tag{4}$$

where T_{e}, T_{gas} and N_A are the electron temperature, gas temperature and Avogadro constant, respectively.

$$k_4 = rei * N_A \tag{5}$$

k_4 is irreversible chemical reaction coefficient of bibody reaction 4, and *rei* is reaction coefficient of electron-positive ion attachment.

$$k_5 = rnp * N_A \tag{6}$$

k_5 is irreversible chemical reaction coefficient of bibody reaction 5, and *rnp* is reaction coefficient of positive and negative ions.

B. IONIC REACTION ON ELECTRODE SURFACE

The positive ion p nearby anode surface will experience neutralization reaction p => A with electron in air corona under normal pressure, and the surface reaction rate is r_p, unit: mol/(s· m^2), and it can be expressed as formula (7) [20]. Ion nearby cathode surface will experience reactions n => A and p => A in air discharge under normal pressure, where positive ion reaction equation on cathode surface is consistent with formula (7). The negative ionic reaction rate on cathode surface is r_n which can be expressed as formula (8) [20].

$$r_p = k_{s,p} c_p \tag{7}$$

$$r_n = k_{s,n} c_n \tag{8}$$

where $k_{s,p}$, c_p, $k_{s,n}$, and c_n, are the anodic reaction equation coefficient, positive ion molar concentrations, cathodic reaction equation coefficient and negative ion molar concentration, respectively.

C. ELECTRON TRANSPORT EQUATION

The electron transport equation in air corona discharge process under normal pressure is described based on electrodynamics collision theory of micro-level Maxwell, probability distribution in consideration of electron migration and diffusion in electric field from macro-level. Its constitutive equation is expressed as formula (9) [19].

$$\frac{\partial}{\partial t} n_e + \nabla \cdot [-n_e (\mu_e \cdot E) - D_e \cdot \nabla n_e] = R_e \tag{9}$$

where n_e, μ_e, E, and D_e, are the spatial electronic number density, electron mobility, electric-field vector and electron diffusion coefficient, respectively. Electron diffusion coefficient D_e is comprehensively influenced by electron temperature and mobility. The relation among the three is [20], [21]:

$$D_e = \mu_0 |k_\mu E|^n T_e \tag{10}$$

where μ_0, k_μ and n are the base electron mobility, electric field linear correction coefficient and nonlinear correction coefficient of electric field, respectively.

In Equation (9), *R*e is algebraic sum of rates of electrons generated or consumed by all ionic reactions contained in reaction 1 to reaction 4 in Table 2. The first term at left side of the equation represents time-dependent change degree of electron number density within any analytical unit. The second term is electron number density inside any non-boundary unit, and it is comprehensively influenced by electric field migration of electrons within its nearby unit and diffusion effect caused by concentration gradient ∇n_e. During the calculation process, in order to couple with traditional Townsend discharge theory and experimental test data, reduced unit is usually used to couple electric field intensity $|E|$ with the electrodynamics collision theory of micro-level Maxwell probability distribution. In the air under normal pressure, the relation between average electron energy in air corona discharge and reduced electric field intensity is experimentally verified as shown in Figure 3 [20]–[23]. This transformation relation can transform electric field intensity solved from macro-level into average electron energy equation, which is then further substituted into transformation relations in Figure 1 and Figure 2 to calculate coefficients of ionic reaction equations (1) to (4) in air corona discharge process. In consideration that the ionization effect triggered by strong electric field in the discharge process will prevent electron migration and movement in the plasma region. Therefore, the electron mobility in formula (9) is corrected into the form with dependence on electric field intensity, and its expression is [20], [21]:

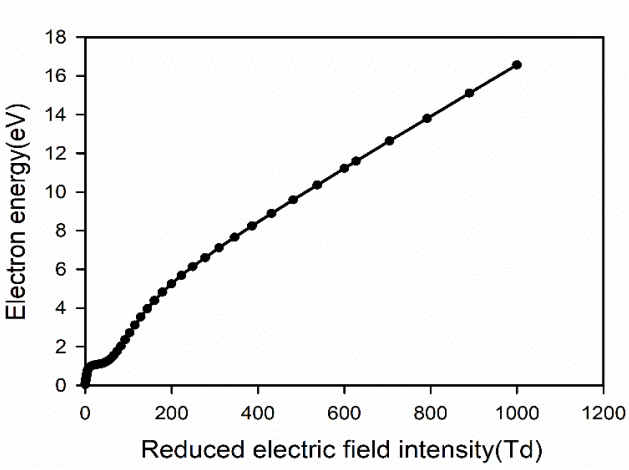

FIGURE 3. Relation curve between average electron energy and reduced electric field intensity in air corona discharge process under normal pressure [22-25].

$$\mu_e = \mu_0 |k_\mu E|^n \tag{11}$$

where n is nonlinear correction coefficient of electric field.

D. TRANSPORT EQUATION OF ELECTRON ENERGY

Electron energy is the macroscopic characterization of the kinetic energy of electron motion. The greater the electron energy, the greater the speed of motion, the easier it is to collide, excite, ionize and react with heavy ions. The electron energy field is similar to the electron concentration and follows the principles of diffusion, convection and electric field migration. The transport equation can be expressed as formula (12) [19].

$$\frac{\partial n_\varepsilon}{\partial t} + \nabla \cdot [-(\mu_\varepsilon \cdot E) n_\varepsilon - \nabla (D_\varepsilon n_\varepsilon)] + E \cdot [-(\mu_\varepsilon \cdot E) n_\varepsilon - \nabla (D_\varepsilon n_\varepsilon)] = S_{en} - (u \cdot \nabla) n_\varepsilon + \frac{Q + Q_{gen}}{q} \tag{12}$$

where n_ε, μ_ε, D_ε, S_{en}, u, Q and Q_{gen} are the electron energy density, electron energy mobility, electron energy diffusivity, energy loss/gain, neutral fluid velocity, external heat source and generalized heat source, respectively.

E. TRANSPORT EQUATION OF HEAVY IONS

Heavy ions refer to other charged particles and neutral particles except for electrons. In the discharge region, their

transport equation can be expressed as formula (13) [16]:

$$\rho \frac{\partial}{\partial t} w_k + \rho \left(\mathrm{u} \cdot \nabla\right) w_k = \nabla \cdot j_k + R_k \tag{13}$$

$$j_k = \rho D_k \nabla w_k + \rho D_k w_k \frac{\nabla M_n}{M_n} + \rho w_k D_k^T \frac{\nabla T}{T} - z_k \mu_k E \tag{14}$$

where w_k, ρ, u, j_k, R_k, D_k, D_k^{T}, M_n, z_k and μ_k are the molar-volume fraction of k-th heavy ion, mixed gas density, flow field velocity, transport vector fluxes of k-th heavy ion in the reaction process, mass consumption and formation rate of k-th heavy ion in ion reaction, diffusion coefficient of k-th heavy ion, thermal diffusion coefficient of k-th heavy ion, molar mass of k-th heavy ion, the number of charge elements of k-th heavy ion and electric mobility of k-th heavy ions, respectively. For a reaction system with multiple heavy ions, this flux is driven by various mechanisms, mainly including diffusion, molecular motion, thermal motion and field-induced migration. The four mechanisms can be expressed as the four right terms in Eq. (14), successively.

F. POISSON'S EQUATION

In air discharge process under normal pressure, electric field E in discharge region is under comprehensive action of potential difference between electrodes and concentration distribution of space charged particles. The spatial electric field distribution follows Gauss theorem of electrostatic field, and its mathematical expression can be expressed by Poisson's equation (15), where the relation between electric field vector E and space potential V is shown in formula (16). The relation between space charge density in formula (15) and number density of space charged particles is shown in formula (17) [16].

$$\nabla \cdot (\varepsilon_0 \varepsilon_r E) = \rho_q \tag{15}$$

$$E = -\nabla V \tag{16}$$

$$\rho_q = e_0 \left(n_p - n_n - n_e\right) \tag{17}$$

where ε_0, ε_r, ρ_{q}, V, n_p, n_n, n_e and e_0 are the permittivity of free space, relative dielectric constant, space charge density, electric potential, positive ion number density, negative ion number density, the number density of space electrons and unit charge quantity, respectively.

III. NUMERICAL SIMULATION

A. GEOMETRIC MODEL USED FOR FEM

Figure 4(a) is the physical picture of discharge device. Finite element model used to describe air corona discharge is constructed according to parameters of actual experimental equipment. Multiphysics finite element simulation software is used to establish a 2D axisymmetric geometric structure for simulating air corona discharge. Figure 4(b) is the geometric model used for FEM.

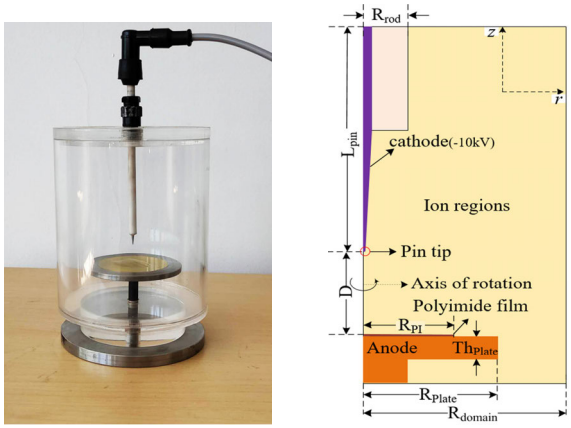

FIGURE 4. (a) Physical picture of discharge device (b) Geometric Model Used for FEM.

B. BOUNDARY CONDITIONS

Boundary condition for metallic contact is constraint of boundary potential V, and its mathematical expression is:

$$V = -V_0 f_{(t)} \tag{18}$$

where $V_0 = 10\mathrm{kV}$, $f_{(\mathrm{t})}$ is time ramp function used to simulate the dynamic process of negative high-voltage power supply climbing to rated negative high-voltage potential since being started. In this simulation, $f_{(t)}$ is ramp function with slope factor being $10^5(1/\mathrm{s})$, where the potential constraining grounding electrode is usually zero, namely

$$V = 0 \tag{19}$$

Zero-charge boundary condition is set at external boundary of ion region to improve the model convergence, and its expression is:

$$D \cdot \mathbf{n} = 0 \tag{20}$$

where D is displacement density ($\mathrm{C/m^2}$), $\mathbf{n}$ is normal vector of dimensionless boundary. The axisymmetric boundary condition is taken as default condition of the 2D axisymmetric finite element model at the position of connecting line of pin electrode and plate electrode center. In consideration that positive ion, negative ion and electron will go through collision, adsorption and neutralization reactions on electrode surface, surface reaction boundary condition should be applied to electrode surface as seen in formulas (7) and (8).

C. PARAMETERS USED IN FINITE ELEMENT SIMULATION

The computational domain of simulation model is shown in Fig. 4(b). The model is a two-dimensional axisymmetric geometric model, and its rotation axis is z axis. The structural parameters of the simulation model set as Table 3. Since the size is too small, polyimide film thickness ($\mathrm{Th_{PI}}$), needle electrode tip radius ($\mathrm{R_{Pin-tip}}$) and needle electrode end radius ($\mathrm{R_{Pin-end}}$) cannot be marked in Fig. 4(b), which value is 0.25 mm, 0.5mm and 2mm respectively. The reaction parameters and environmental parameters of the simulation model

TABLE 3. Structural parameters of the simulation model.

Variable name	Values (mm)	Variable description
R_{PI}	20	Radius of polyimide film
Th_{PI}	0.25	Thickness of polyimide film
R_{rod}	10	External diameter of rod electrode
L_{pin}	55	Length of rod electrode
R_{Plate}	30	Radius of plate electrode
Th_{Plate}	5	Thickness of plate electrode
D	20	Distance of Pin-plate electrode
R_{domain}	45	Radius of air region
$R_{Pin\text{-}tip}$	0.5	Radius of pin-tip
$R_{Pin\text{-}end}$	2	Radius of pin-end

TABLE 4. Reaction parameters and environmental parameters.

Parameters	Values/units	Parameters description
μ_N	6E20[1/(V·s·m)]	Reduction mobility of ion
r_{np}	2E-6 [cm^3/s]	Reaction coefficient of positive-negative ions
r_{ei}	5E-8 [cm^3/s]	Reaction coefficient of electron-positive ion attachment
ni_0	1E8 [1/m^3]	Initial ion density
Ne_0	1E10 [1/m^3]	Initial electron density
Temp	20°C	Ambient temperature
Pre	760[torr]	Ambient pressure
Hum	30%	Relative humidity of air

TABLE 5. Material property parameter.

Materials	Values/units	Parameters description
Copper	8960[kg/m^3]	ρ_C(Copper density)
	385[J/(kg·K)]	$C_{P\text{-}C}$(Mass heat capacity of copper)
	400[W/(m·K)]	K_C(Thermal conductivity of copper)
Polyimide	1420[kg/m^3]	ρ_{PI}(Density of polyimide)
	1090[J/(kg·K)]	$C_{P\text{-}PI}$(Mass heat capacity of polyimide)
	1.2[W/(m·K)]	K_{PI}(Thermal conductivity of polyimide)
	2.5	$\varepsilon_{r\text{-}PI}$(Relative permittivity of polyimide)
Air	1	ε_r(Relative permittivity of air)

set as Table 4. This simulation model involves four materials, namely copper, polyimide, air and ceramics. The material property parameter set as Table 5. Due to space constraints, the above table lists only a small number of simulation parameters.

D. DISTRIBUTION OF SPACE POTENTIAL AND ELECTRIC FIELD

The space potential distributions in initial stage (10μs), intermediate stage (0.1ms) and final stage (3.7ms) of corona discharge are shown in Fig. 5(a), 5(b) and 5(c), respectively. Fig. 5(a) shows space potential distribution when negative high-voltage electrode just reaches -10 kV, when charged ion transport in discharge space has not reached quasi-equilibrium state, and time-dependent potential change degree nearby electrode point is the highest; At 0.1 ms as shown in Fig. 5(b), space potential distribution is changed due to migration and diffusion of charged ions; At 3.7ms as shown in Fig. 5 (c), corona discharge reaches quasi-equilibrium state, as distribution of charged ions tends to be quasi-stable, space potential distribution is more uniform and reaches quasi-stable state.

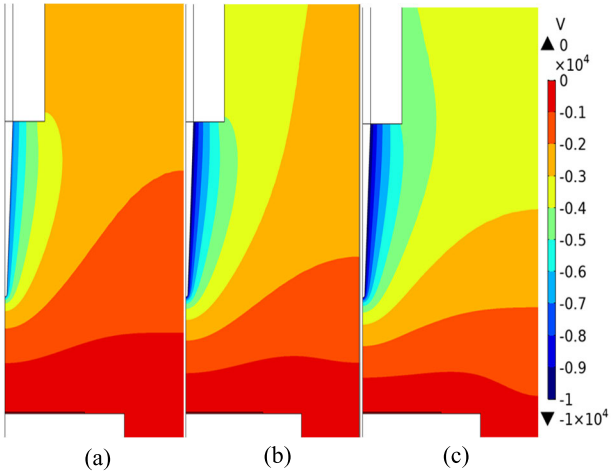

FIGURE 5. Spatial potential distribution in different stages of corona discharge process. (a) t=10μs. (b) t=0.1ms. (c) t=3.7ms.

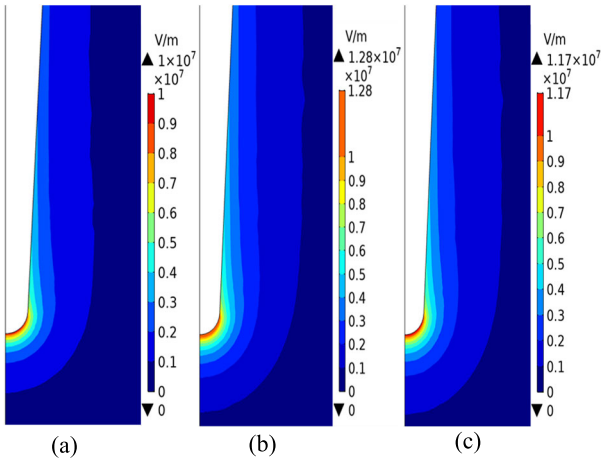

FIGURE 6. Electric field distribution near needle electrode in different stages of corona discharge process. (a) t=10μs. (b) t=0.1ms. (c) t=3.7ms.

Fig 6 (a), 6 (b) and 6 (c) give electric field intensity distributions near negative high-voltage electrode surface at 10μs, 0.1ms and 3.7ms, respectively. As high curvature exists at negative high-voltage electrode tip, local electric field enhancement at tip. During the process from voltage application to formation of steady corona discharge, electric field intensity nearby high-voltage electrode surface changes with time due to space ion transport mechanism, and it gradually reaches a quasi-equilibrium state. Fig 7 shows time-dependent change curve of surface field intensity $|E|$ on negative high-voltage electrode tip. Electric field strength up to 10^7V/m near needle electrode tip. In the curve, the initial abrupt rising trend is contributed by ramp voltage function. When reaching the highest electric field intensity, the charge gathered near the negative electrode surface has not yet migrated and diffused into the whole space. As time passes by, charges on electrode surface are migrated and diffused step by step, and the electric field intensity gradually decreases, but the electric field near the tip of the needle

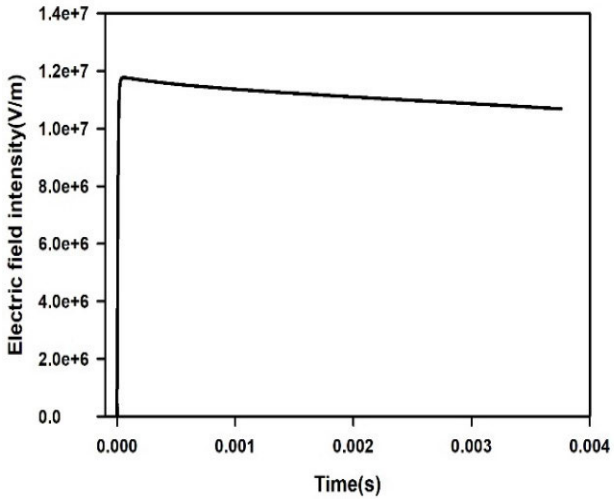

FIGURE 7. The curve of electric field intensity |E| on the tip of negative high voltage electrode varies with time.

electrode is always above 10^7V/m. The distribution of electric field is slightly different from other literatures, which may be due to many factors, such as insulation film materials and thickness, electrode structure and so on.

E. EVOLUTION LAWS OF SPACE CHARGE DISTRIBUTION

Figures 8(a), 8(b), and 8(c) give space charge density distribution cloud pictures at 10μs, 0.1ms and 3.7ms, respectively. In these figures, deep red colour represents positive charge, dark blue colour is negative charge. In initial and intermediate stages of corona discharge, high-concentration charge accumulation is generated nearby both negative high-voltage electrode and grounding electrode, and accumulation concentration is higher where the curvature is greater. Positive and negative charges present alternate distribution in nearby space of electrode. As time passes by, positive charge is migrated towards negative high-voltage electrode while negative charge moves towards grounding electrode, finally reaching quasi-equilibrium state. After electron avalanche takes place, electrons are migrated towards ground electrode under the action of electric field force and accumulated in head region of corona development, so they present dark blue lamellar distribution state. The rest positive ions almost don't change in spatial position due to their large mass so as to fill the region where ionization takes place between pin-plate electrodes and draw close to high-voltage cathode space. Positive and negative charges present alternate distribution in initial corona discharge stage and during the discharge process, which is rightly the result of continuous advancement of electron avalanches towards ground electrode. After the quasi-stable state is reached in the end, a large number of positive ions are left nearby high-voltage cathode, only a large number of negative charges are accumulated nearby ground electrode, so quasi-equilibrium charge distribution is decided mainly by electric field.

Figures 9(a) and 9(b) give logarithmic distribution cloud pictures of molar fractions of positive ions and negative ions between point-plate electrodes when corona discharge reaches a quasi-stable state at 3.7ms. Figure 9(c) give logarithmic distribution cloud pictures of electron number density between point-plate electrodes when corona discharge reaches a quasi-stable state at 3.7ms. The arrows in Figures 9 indicates the fluxes of Positive ion, Negative ion, Electrons, respectively.

As concentration order of space charged particles in discharge space is large, 10-based logarithm is used for data processing and plot drawing. It can be found through Figure 9(a) that the concentration of positive ions nearby ground electrode is the lowest when corona discharge reaches a quasi-stable state, and the transport direction is turned from ground electrode to negative high-voltage pin electrode;

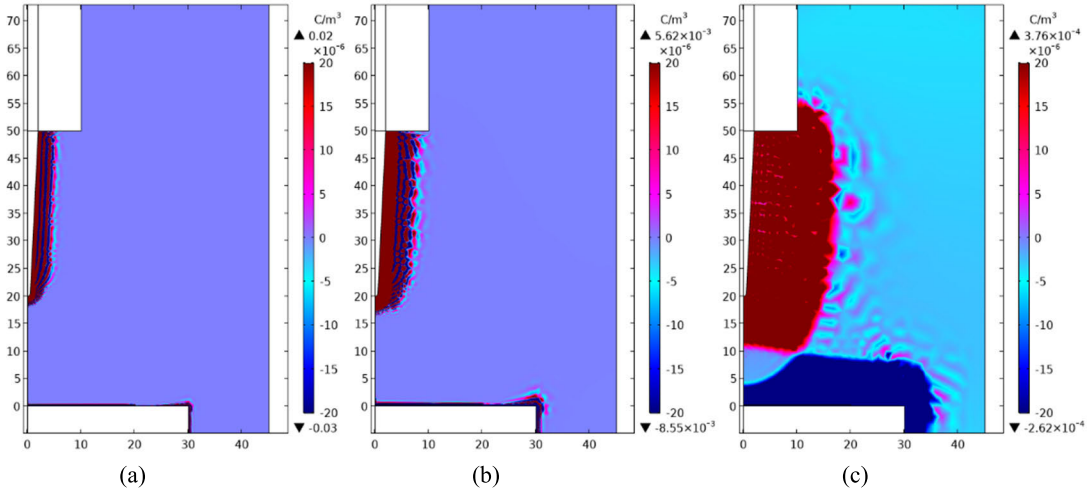

FIGURE 8. Distribution of space charge density in different stages of corona discharge process. (a) t=10μs (b) t=0.1ms (c) t=3.7ms.

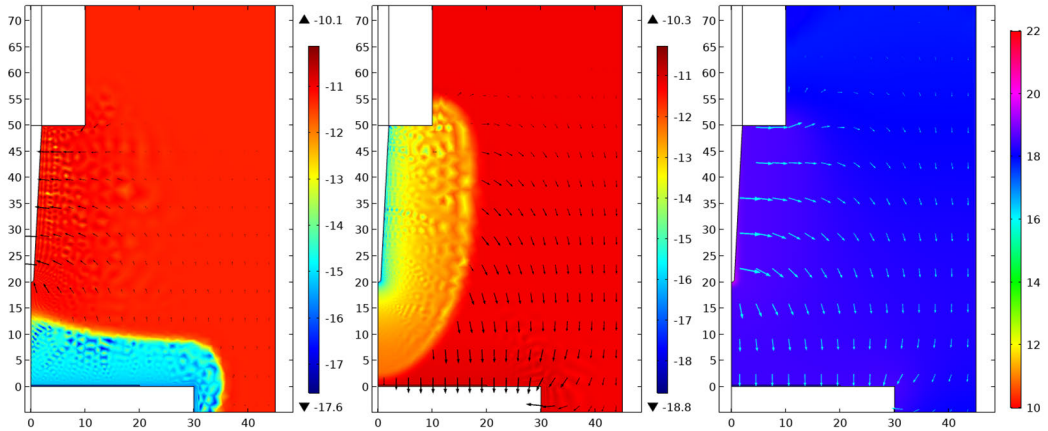

FIGURE 9. Cloud image of density distribution of positive ions, negative ions and space electrons in quasi-stable state of corona discharge (a) Log(Positive ion mole fraction, 1) (b) Log(Negative ion mole fraction,1) (c) Log(Electronic number density, $1/m^3$). The arrows indicates the fluxes direction of Positive ion, Negative ion and Electrons, respectively.

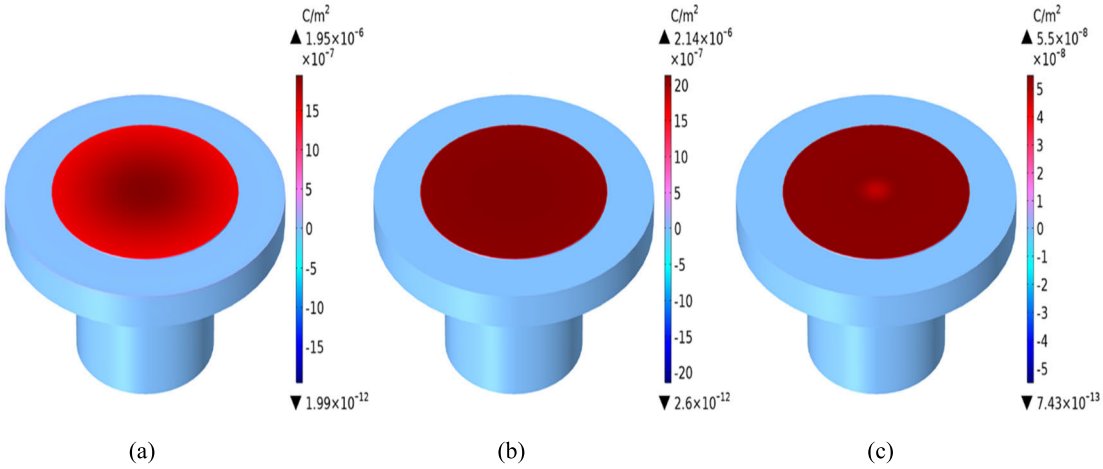

FIGURE 10. Distribution of the charge density (C/m^2) of the polyimide surface at different time in the corona charge process.(a) t=10μs (b) t=0.1ms (c) t=3.7m.

On the contrary, the concentration of negative ions nearby negative high-voltage pin electrode is the lowest in Figure 9(b), and the transport direction is turned from negative high-voltage pin electrode to ground electrode. It can be seen from Figure 9(c) that electrons fill the space between pin-plate electrodes, the concentration at electrode tip with the largest curvature is the highest, and the electron transport direction is from negative high-voltage pin electrode and reaches ground electrode under the action of electric field migration.

Figures 10(a), 10(b), and 10(c) give charge density distribution cloud pictures of polyimide surface obtained by the revolution of the 2-D symmetric numeric model at 10μs, 0.1ms and 3.7ms, respectively. Figure 10(a) is corresponding to initial corona discharge stage, charge density in film central region is obviously higher than that in marginal region, and this result can be explained like this: electrons released at negative high-voltage cathode in the initial stage take the lead to arrive at the center of ground electrode surface covered by polyimide film, so the charge concentration on the surface of central region is the highest. Through electric field migration for a certain time, charge distribution is as shown in Figure 10(b) in intermediate stage of corona discharge. Electrons produced by corona discharge reach the insulated film surface in succession and present relatively uniform surface charge density on the surface. When corona discharge reaches a quasi-stable state, the surface charge density in central region of the film is gradually lowered due to mutual repulsion of surface charges and migrating effect of surface electric fields on surface charges as shown in Figure 10c.

F. CHARGE ACCUMULATION CHARACTERISTICS AND EVOLUTION LAWS

Figure 11 gives the charge density distribution curves on the line segment (radius) from the center of polyimide film circle to margin at 10μs, 0.1ms and 3.7ms, respectively. 10μs curve

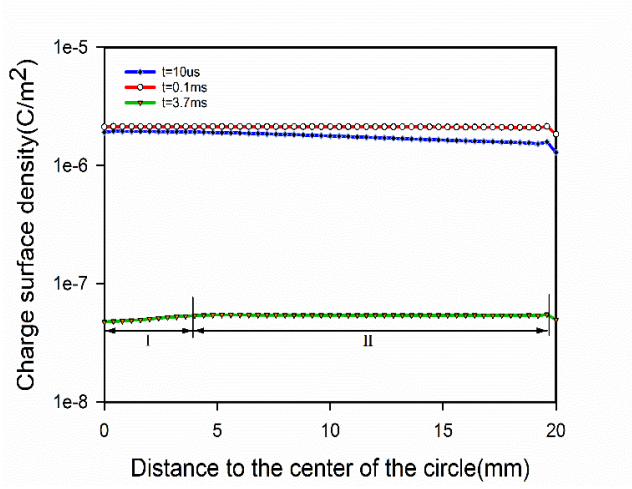

FIGURE 11. Surface charge density distribution curves on the line segment from center of polyimide film circle to margin (t=10μs, 0.1ms, 3.7ms).

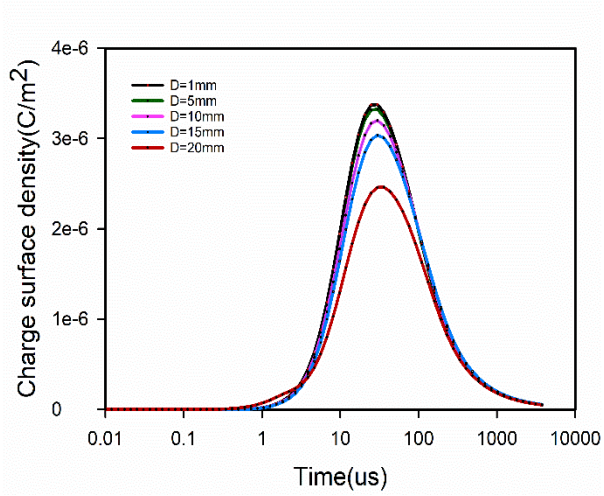

FIGURE 12. Time-dependent curves of surface charge density at D (D=1mm, 5mm, 10mm, 15mm, 20mm) from center of circle.

in Figure 11 clearly displays no uniformity degree of surface charge density distribution in initial corona discharge stage, where the charge density is the highest in central region of polyimide film. As the distance from the center of circle increases, the surface charge density gradually declines. The 0.1ms curve in Figure 11 is corresponding to intermediate corona discharge stage, and it can be seen that as the distance from the center of circle increases, the surface charge density changes little and the charge density distribution is quite uniform. The 3.7ms curve in Figure 11 is corresponding to quasi-stable stage of corona discharge, and it can be seen that the surface charge density is the minimum at the center of circle. As the distance from the center of circle increases, the surface charge density gradually increases (region I). After the distance reaches about 5 mm, the surface charge density distribution becomes uniform (region II). Through an observation by combining Figure 11 and Figures 10, comprehensive and clear surface charge density distribution laws in different corona discharge stages can be acquired.

It can be seen from Figure 11 that the surface charge density reaches 10^{-6}C/m^2 order of magnitudes in initial and intermediate corona discharge stages, and it reaches 10^{-8}C/m^2 under quasi-stable state. This is because in initial and intermediate corona discharge stages, a large number of these positive ions, negative ions and electrons generated by ionization are accumulated on the polyimide surface, it's too late for charges of different polarity to be fully neutralized. A large number of charged particles of different polarity are already neutralized under quasi-stable state and reach quasi-equilibrium of ionization and neutralization reactions, all kinds of charged ions are reduced sharply, and the main charge components are remaining electrons, so the surface charge density is much smaller under quasi-stable state.

Figure 12 gives the time-dependent change curves of surface charge densities when the distance D from the center of circle is 1mm, 5mm, 10mm, 15mm and 20mm, respectively. Obviously, at different distances from the center of circle, the time-dependent change curves of surface charge density have the same development trend with quadratic curve unimodal form, the surface charge density reaches peak value (10^{-6}C/m^2) within dozens of microseconds and then slowly declines and finally is stabilized at 10^{-8} C/m^2 in a few milliseconds. As the distance from the center of circle increases, the maximum surface charge density is reduced and the time for it to reach peak value is postponed. This is because in the corona discharge process, a large number of charged ions take the lead to reach the polyimide film center and its nearby position. In the position away from the center, a significant part of the accumulated charge were migrated from the central area under the action of the electric field force, so the closer to the center, the earlier the peak value will be reached, and the farther from the center, the smaller the peak value.

G. TEMPORAL EVOLUTION LAWS OF TOTAL CHARGE NUMBER ON POLYIMIDE SURFACE

Integral of charge densities on polyimide surface at different time is taken, and the time-varying curves of total surface charge number can be obtained as shown in Figure 13. In order to clearly display the charge accumulation process in initial stage, logarithmic form is taken for horizontal axis of time in the figure. It can be seen that the charge accumulation process within the first 30 μs is mainly because ionization degree is continuously elevated in the rising zone of voltage ramp function, and more charged particles are accumulated on the surface of insulation material. As the simulation time continues to increase, charged ions like electrons, positive ions and negative ions ionized out in the initial stage are migrated under the action of electric field, accompanied by ionic reactions such as adsorption and neutralizationin the meantime. After ''a long enough time'', consumption and

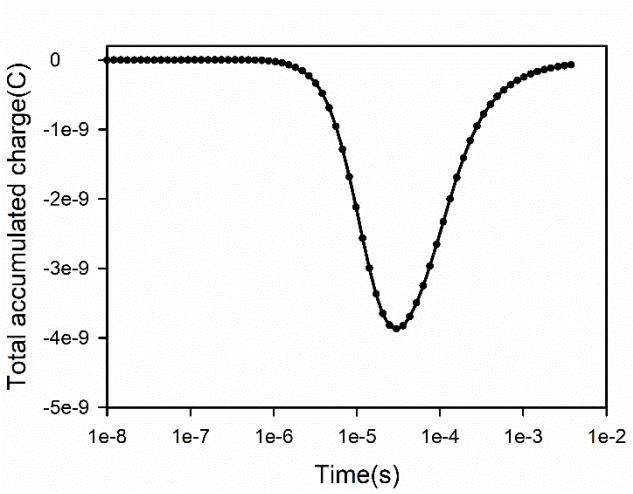

FIGURE 13. Total surface charge number-time relation curve.

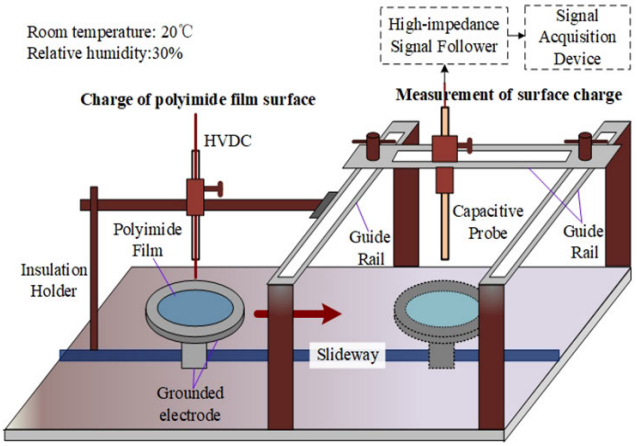

FIGURE 14. Insulation film charge accumulation and charge density test platform.

yield of ions in the reactions reach quasi-equilibrium state, and total charge number on polyimide surface tends to be balanced. Under this simulation condition, total number of charges accumulated on the surface is at 10^{-10} Coulomb order in quasi-equilibrium state.

IV. EXPERIMENTAL VERIFICATION

A. EXPERIMENTAL DEVICE

Figure 14 shows structural diagram of experimental device. The left side is charged part of insulated film and the right side is charge test part, and ground electrode is installed on the track. The device of charged part consists of two parts: high-voltage pin electrode, which can adjust horizontal and vertical positions, installed on insulated beam; ground electrode installed on the track. The device of charge test part consists of three parts: capacity test probe, precision guide rail and signal acquisition processer, where three precisely adjustable guide rails ensure that the charge test probe can precisely adjust the test position in 3D space. The test principle of charge refers to references [24], [25]. Polyimide film can be slid to right side after the left side is charged for surface charge test. The experiment is conducted under ambient temperature of 20° and relative air humidity of 30%. DC high voltage is set at negative 10 kV, and drift current value can be read through a digital microammeter.

B. DISTRIBUTION LAWS OF CHARGE DENSITY ALONG RADIUS UNDER QUASI-STABLE STAT

After negative 10 kV voltage corona discharge and polyimide film charge for 1 min, the surface charge density is tested at test points every other 4 mm from the center of circle along the radius (as the last test point rightly falls at the edge of circumference, it's difficult to accurately measure the charge at this position, and the last test point is selected at 2 mm position at inner side of circumference). Figure15 gives the contrast curves of simulation result and experimental result

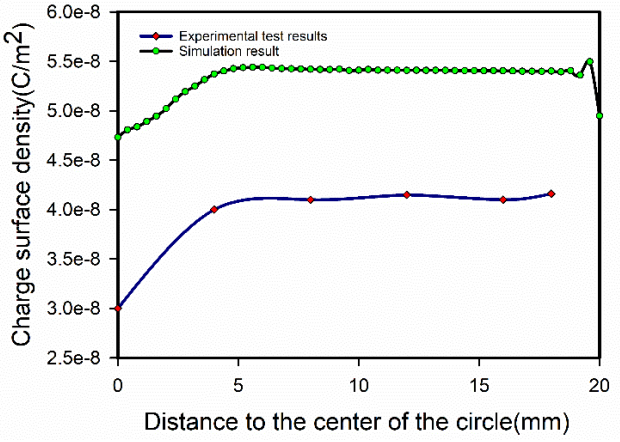

FIGURE 15. Distribution curve of charge density along radius under quasi-stable state.

of surface charge density distribution along radius under quasi-stable state corona discharge process. The two share similar distribution laws, the charge density is small nearby the center of circle, and as the distance from the center of circle increases, surface charge density gradually increases. After the distance from the center of circle is greater than 4 mm, the charge distribution becomes uniform. The measured value is smaller than simulation result, mainly because charge leakage appears since the polyimide charge is completed until the charge test is started and in middle of the test. The surface charge density is slightly increased due to fringe effect nearby the circumference.

C. DRIFT CURRENT TEST UNDER QUASI-STABLE STATE

It can be known from simulation computation that 3.7ms after the corona discharge, the quasi-stable state is reached. Within 1 min after the corona discharge and since the voltage is applied, drift current value is read from the microammeter every other 10s. Figure 16 gives the contrast drift current curves of simulation computation (red line) and experimental

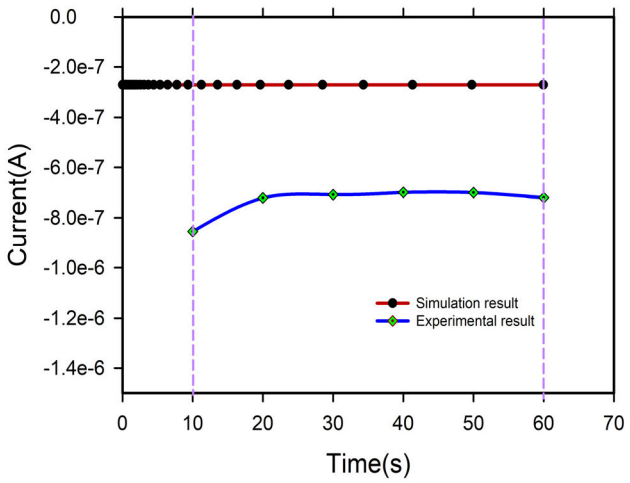

FIGURE 16. **Drift current-time curve at quasi-stable state of corona discharge.**

test (blue line) under quasi-stable state. The experimental test drift current curve is a slightly fluctuating curve, and the current value is about 0.7μA. In order to compare with experimental results, the simulation drift current data time range from 3.7ms to 60 s in figure 16, which is a part of simulation computation result when the quasi-stable state is approached. In order to speed up the calculation progress and reduce the calculation amount, the time step of simulation calculation is increased in proportion. The drift current value of simulation and experimental test are of the same order of magnitude and have similar fluctuation characteristics in the time range of 1s to 60s (both are basically straight lines). It can be seen that simulation result of drift current under quasi-stable state is basically identical with that obtained through the experimental test.

Based on the test of charge density and drift current under quasi-stable state and a comparison with simulation results, the experimental conclusion is basically consistent with the simulation result, thus verifying the correctness of the proposed numerical simulation method and its simulation result indirectly.

V. CONCLUSIONS

The charge accumulation mechanism on polyimide insulating medium in negative high-voltage corona discharge was investigated through numerical simulation. According to the parameters and operating conditions of the established experimental system, a universal 2D axisymmetric model was constructed based on micro-macro coupling plasma reaction equation and transport equation to investigate the charge process of corona polarization insulated surface. A coupling bridge between the micro-ion reaction system and the macroscopic multi-physical field was constructed by means of the electronic energy distribution function, which revealed the coupling mechanism in the process of corona charge. The generation, migration and distribution laws of charged ions and electrons in different stages of corona discharge process were given. Charge distribution laws in different stages of charge process of polyimide were given and discussed. The following items were concluded:

(1) The spatial distribution of electric potential and electric field between electrodes of needle-plate is obtained by simulation. Electric field strength up to 10^7V/m near needle electrode tip.

(2) The distribution of space charge density in different discharge stages is obtained by simulation. In initial and intermediate corona discharge stages, high-concentration charge accumulation is generated nearby both negative high-voltage electrode and ground electrode, and the accumulation concentration is higher where the curvature is greater. Positive and negative charges present alternate distribution nearby the high-voltage electrode at initial time of corona discharge and in the discharge process. After the quasi-stable state is reached in the end, only a large number of positive ions are left nearby the high-voltage cathode, while only a large number of negative charges are accumulated nearby the ground electrode.

(3) The distribution characteristics of polyimide surface charge density and its variation with time are obtained by simulation. In the initial corona discharge stage, the charge density in the central region of insulated film is remarkably higher than that in marginal region. In the intermediate corona discharge stage, relatively uniform surface charge density is presented. When the corona discharge reaches a quasi-stable state, the surface charge density in the central region of the film is lower than that in surrounding region.

(4) The surface charge density is at 10^{-6}C/m^2 order of magnitudes in initial and intermediate corona discharge stages, and it reaches 10^{-8} C/m^2 order under quasi-stable state.

(5) As the distance from the center of circle increases, the maximum surface charge density is reduced and the time for it to reach peak value is postponed.

(6) The curve of the total charge number of polyimide surface with time is given. Under quasi-equilibrium state of corona discharge, the total number of charges accumulated on the surface reaches 10^{-10} Coulomb order of magnitudes.

(7) Based on the test of charge density and drift current in quasi-stable state and compared with the simulation results, the correctness of the proposed numerical simulation method and its simulation results are indirectly verified.

This study is expected to provide theoretical support for the leading mechanism to prevent discharge or flashover along the surface. The effects of materials, humidity and temperature on the discharge process and charge accumulation behavior will be discussed in subsequent studies.

REFERENCES

[1] C. W. Mangelsdorf and C. M. Cooke, "Bulk charging of epoxy insulation under DC stress," in *Proc. IEEE Int. Conf. Electr. Insul.*, Jun. 1980, pp. 146–149.

[2] T. Nitta and K. Nakanishi, "Charge accumulation on insulating spacers for HVDC GIS," *IEEE Trans. Electr. Insul.*, vol. 26, no. 3, pp. 418–427, Jun. 1991.

[3] V. M. Moreno-Villa, M. A. Ponce-Velez, E. Valle-Jaime, and J. L. Fierro-Chavez, "Effect of surface charge on hydrophobicity levels of insulating materials," *Gener., Transmiss. Distrib.*, vol. 145, no. 6, pp. 675–681, Nov. 1998.
[4] A. H. Bonnett, "A comparison between insulation systems available for PWM inverter fed motors," in *Proc. IAS Petroleum Chem. Ind. Tech. Conf.*, Sep. 1996, pp. 49–60.
[5] D.-H. Hwang, D.-Y. Park, Y.-J. Kim, D.-H. Kim, J.-Y. Koo, and I.-G. Hur, "Analysis of insulation characteristics of PWM inverter-fed induction motors," in *Proc. ISIE IEEE Int. Symp. Ind. Electron.*, Jun. 2001, pp. 477–481.
[6] R. Benato, C. Di Mario, and H. Koch, "High capability applications of long gas-insulated lines in structures," in *Proc. PES TD*, May 2006, pp. 605–612.
[7] H. Fujinami, T. Takuma, M. Yashima, and T. Kawamoto, "Mechanism of the charge accumulation and insulation characteristics of gas insulated spacer under DC stress," *IEEJ Trans. Power Energy*, vol. 108, no. 7, pp. 297–304, 1988.
[8] B. Zhang, Q. Wang, Z. Qi, and G. Zhang, "Measurement method and accumulation characteristics of surface charge distribution on polymeric material under DC voltage," *Proc. CSEE* vol. 36, no. 24, pp. 6664–6676, 2016.
[9] T. Sumita, T. Yamaki, S. Yamamoto, and A. Miyashita, "Photo-induced surface charge separation of highly oriented TiO2 anatase and rutile thin films," *Appl. Surf. Sci.*, vol. 200, nos. 1–4, pp. 21–26, Nov. 2002.
[10] H. T. Baytekin, A. Z. Patashinski, M. Branicki, B. Baytekin, S. Soh, and B. A. Grzybowski, "The mosaic of surface charge in contact electrification," *Science*, vol. 333, no. 6040, pp. 308–312, Jul. 2011.
[11] F. Wang, Q. Zhang, Y. Qiu, and E. Kuffel, "Insulator surface charge accumulation under DC voltage," in *Proc. Conf. Rec. the IEEE Int. Symp. Electr. Insul.*, Apr. 2002, pp. 426–429.
[12] F. Wang, Y. Qiu, W. Pfeiffer, and E. Kuffel, "Insulator surface charge accumulation under impulse voltage," *IEEE Trans. Dielectr. Electr. Insul.*, vol. 11, no. 5, pp. 847–854, Oct. 2004.
[13] V. M. Moreno and R. S. Gorur, "AC and DC performance of polymeric housing materials for HV outdoor insulators," *IEEE Trans. Dielectr. Electr. Insul.*, vol. 6, no. 3, pp. 342–350, Jun. 1999.
[14] Y. Liu, Z. An, J. Cang, Y. Zhang, and F. Zheng, "Significant suppression of surface charge accumulation on epoxy resin by direct fluorination," *IEEE Trans. Dielectr. Electr. Insul.*, vol. 19, no. 4, pp. 1143–1150, Aug. 2012.
[15] J. Wu, L. Lan, X. Li, and Y. Yin, "The influence of nano-filler on space charge distribution in LDPE/silica nanocomposites," in *Proc. Int. Symp. Electr. Insulating Mater.*, Sep. 2011, pp. 341–344.
[16] B. M. Smirnov, *Theory of Gas Discharge Plasma*. Springer, 2015.
[17] Zhang, Jian, B. K. Zhu, and Y. Y. Xu, "Characterization and dielectric property of polyimide-silica composite films prepared via sol-gel and thermal imidization process," *J. Mater. Sci.*, vol. 40, nos. 9–10, pp. 2623–2625, 2005.
[18] Y. Jinji, *Gas Discharge*. Beijing, China: Cui Jian, 1983, pp. 43–44.
[19] H. Liang, B. Du, J. Li, and Q. Du, "Numerical simulation on the surface charge accumulation process of epoxy insulator under needle-plane corona discharge in air," *IET Sci. Meas. Technol.*, vol. 12, no. 1, pp. 9–16, 2018.
[20] M. A. Lieberman and A. J. Lichtenberg, *Principles of Plasma Discharges and Material Processing*, 2nd ed. Hoboken, NJ, USA: Wiley, 2005, p. 800.
[21] *Low Temperature Plasma Data Exchange Project Website*. Accessed: Oct. 10, 2019. [Online]. Available: https://fr.lxcat.net/home/
[22] A. Kulikovsky, "Positive streamer between parallel plate electrodes in atmospheric pressure air," *J. Phys. D, Appl. Phys.*, vol. 30, no. 30, p. 441, Feb. 1997.
[23] V. A. Godyak, R. B. Piejak, and B. M. Alexandrovich, "Electron energy distribution function measurements and plasma parameters in inductively coupled argon plasma," *Plasma Sour. Sci. Technol.*, vol. 11, no. 4, pp. 525–543, Nov. 2002.
[24] B. Qi, C. Gao, C. Li, L. Zhao, and X. Sun, "Effect of surface charge accumulation on flashover voltage of GIS insulator in SF6 under DC and AC voltages," in *Proc. IEEE Conf. Electr. Insul. Dielectr. Phenomena (CEIDP)*, Oct. 2015, pp. 848–851.
[25] S. Tenbohlen and G. Schroder, "The influence of surface charge on lightning impulse breakdown of spacers in SF_6," *IEEE Trans. Dielectr. Elect.* vol. 7, no. 2, pp. 241–246, Apr. 2000.

TAO FENG received the B.Eng. and M.Eng. degrees in electrical engineering from Shijiazhuang Tiedao University, China, in 2003 and 2010, respectively. He is currently pursuing the Ph.D. degree with the State Key Laboratory of Power Transmission Equipment and System Security and New Technology, Chongqing University.

He is also a Teacher with the College of Electrical Engineering, Shijiazhuang Tiedao University. His research interests include prebreakdown and breakdown properties of gas and liquid insulation, insulation ageing, and alternative insulation materials for transformers.

WEI HE was born in China, in 1957. He received the Ph.D. degree from the Hamburg University of Technology, in 1997.

He is currently a Professor with the Department of Electrical Engineering, Chongqing University, China. He is the author of more than 100 journal articles. His research interests include measurement, calculation, and ecological effects of electromagnetic field in ultrahigh voltage environment and bio-electromagnetic induction imaging.

JIN GANG WANG received the B.Eng., M.Eng., and Ph.D. degrees in electrical engineering from Chongqing University, China, in 2001, 2003, and 2008, respectively.

He is currently a Professor with the Department of Electrical Engineering, Chongqing University. His research interests include calculation, measurement, and application of electromagnetic field, weak signal measurement and processing, and detection of high-voltage equipment discharge.